Journal of The Electrochemical Society, 2021 **168** 060548
1945-7111/2021/168(6)/060548/10/$40.00 © 2021 The Electrochemical Society (“ECS”). Published on behalf of ECS by IOP Publishing Limited

Fast Charging of Energy-Dense Lithium Metal Batteries in Localized Ether-Based Highly Concentrated Electrolytes

Yongjun Leng, Shanhai Ge, Xiao-Guang Yang, Ryan S. Longchamps,[*] Teng Liu,[*] and Chao-Yang Wang[,z]**

Electrochemical Engine Center and Department of Mechanical Engineering, Pennsylvania State University, University Park, PA 16802, United States of America

Li metal batteries (LMBs) employing high voltage cathodes show promise as next generation batteries for electric vehicles due to their high energy density. However, the cycling stability of such energy-dense LMBs at high charge rates has seldom been explored. In this work, Li Coulombic efficiency (CE) as a function of current density (i.e., C-rate) and temperature was investigated in ether-based highly concentrated electrolytes (HCEs). We found that Li metal anodes can be stably cycled in the HCEs at elevated temperatures with a high Li CE of >99.4% for a plating capacity of 3 mAh cm^{-2} at a high C-rate greater than 1 C. The cycling stability of LMB full cells with $Li(Ni_{0.8}Co_{0.1}Mn_{0.1})O_2$ (NMC811) cathodes was also investigated at different charge rates (1 C to 3 C) at 40 and 60 °C. The LMBs with high areal capacity (~3.2 mAh cm^{-2}) NMC811 cathodes and minimal Li excess anodes (negative/positive capacity ratio (N/P ratio) <3.1) can achieve ~189 stable cycles with an average efficiency of ~99.86% at 1 C charge and C/3 discharge at 60 °C.

[DOI: 10.1149/1945-7111/ac0bf3]

Manuscript submitted March 6, 2021; revised manuscript received May 12, 2021. Published June 24, 2021.

Supplementary material for this article is available online

Range anxiety is a major obstacle hindering acceptance of battery-powered electric vehicles (EVs) by consumers.[1–4] The effective strategies to alleviate this anxiety include increasing the energy density of the batteries[4] and/or providing the consumers with extremely fast (⩽10 min) and convenient charging.[3,5] To boost battery specific energy beyond that of state-of-the-art Li ion batteries with graphite anodes to above 300 Wh kg^{-1}, development of next-generation batteries with high capacity anode and/or cathode materials is required. Lithium (Li) metal has been regarded as the most promising anode material for next-generation batteries since it has the lowest electrochemical potential (−3.04 V vs standard hydrogen electrode (SHE)) as well as a theoretical capacity as high as 3,860 mAh g^{-1}.[6–8] However, there are several challenges that impede the practical use of Li metal anodes, including low Coulombic efficiency (CE) due to parasitic reactions between Li metals and liquid electrolytes as well as uncontrolled Li dendrite formation/growth which may cause internal shorting and safety issues.[8–10]

During the past decade, Li metal batteries (LMBs) with Li metal as the anodes have been extensively studied and many strategies have been developed with focus on increasing the Li CE and/or suppressing the formation/growth of Li dendrites.[7–11] The strategies reported in the literature include Li surface protection,[12–14] three dimensional host/matrix implementation,[15–19] Li alloying with other elements,[20–22] modification of liquid electrolyte formula,[23–28] adoption of highly concentrated electrolytes,[11,29–42] and the use of solid electrolytes.[15,43–46] Among these strategies, highly concentrated electrolytes (HCEs) have attracted much attention.[32–42,47] In HCEs, the Li metal anode can be stably cycled with a high Li CE due to the solvation of a majority of the initial solvent with Li ions, leaving a small free solvent fraction. This strategically reduces the parasitic reaction between Li metal and free solvents.[11,48] Moreover, Li dendrite formation/growth can be effectively suppressed by the robust, LiF-rich solid-electrolyte interphase (SEI) layer formed on the Li surface in HCEs, which is derived from the reduction of salts rather than solvents.[11,48] Most recently we demonstrated that an ether-based HCEs (such as 3–5 M lithium bis(fluorosulfonyl)imide (LiFSI) dissolved in 1,2-dimethoxyethane (DME)) can enable stable operation of LMBs with high-voltage layered oxide cathodes such as $LiNi_{0.6}Mn_{0.2}Co_{0.2}O_2$ (NMC622) at room temperature and elevated temperatures.[4] In our work, LMBs with NMC622 cathodes and minimal excess Li metal anodes (negative/positive capacity (N/P) ratio of only 2.12) have been cycled for 200–300 cycles at 60 °C in ether-based HCEs. Pouch cells designed based on the same cell components as the coin cells reported in our work are expected to have an energy density of ~250 Wh kg^{-1}.[4] As an extension of the HCE approach, the introduction of inert diluents, which reduce the electrolyte viscosity to yield so-called localized HCEs, has been previously reported by other groups.[41,49,50] For example, Chen et al.[41] reported a localized HCE such as 1.2 M LiFSI dissolved in a mixture of dimethyl carbonate (DMC) and bis(2, 2, 2-trifluoroethyl) ether (BTFE) (DMC/BTFE = 1:2 by mol) that enables dendrite-free cycling of lithium-metal anodes with high Coulombic efficiency (99.5%) and excellent cycling stability of Li || $LiNi_{1/3}Mn_{1/3}Co_{1/3}O_2$ (NMC333) batteries.

Beyond high Li CE and dendrite-free cycling, high energy-density is equally critical to practical LMB development. LMBs reported in the literature often adopt very thick (⩾250 μm) Li anodes containing more than an order of magnitude of Li greater than the amount actually being cycled, which significantly reduce the energy density of LMBs.[4,6,51,52] Such LMBs cannot be implemented for practical use since they cannot achieve high practical energy density.[4] Recently, much effort has been dedicated to developing energy-dense LMBs (⩾300 Wh kg^{-1}) by minimizing the excess amount of the Li metal anode (N/P ration ⩽3), and adopting high voltage and high areal capacity cathodes, and/or reducing the amount of non-active components.[6,18,28,37,50,52–54]

As mentioned, fast charging of energy-dense batteries offers a complementary solution to range limitations in automotive batteries. In the literature, there are a few reports on cycling stability of LMBs under fast-charging conditions (i.e., at a high charge C-rate).[55–57] For example, Lu et al.[55] investigated the effect of charge rate (from 0.2 C to 4 C) on the cycling behavior of LMBs with 0.45 mm thick Li chips and $Li(Ni_{0.85}Co_{0.10}Al_{0.05})O_2$ (NCA) cathodes with a areal capacity of 2 mAh cm^{-2} in conventional liquid electrolytes such as 1 M $LiPF_6$ in EC/EMC (4:6 by weight). It was found that increasing charge C-rate from 0.2 C to above 1 C significantly reduces the cycle life from >200 cycles to <20 cycles, in spite of the thick Li foil used in the cell. They believed that at high current densities (i.e., high C-rate), the quick formation of highly resistive SEI layer entangled with Li metal, which grows towards the bulk Li, dramatically increases the cell impedance and serves as the origin of cell degradation and failure. Zheng et al.[57] demonstrated that a Li metal

---

[*] Electrochemical Society Student Member.
[**] Electrochemical Society Member.
[z] E-mail: cxw31@psu.edu

battery with a thick Li foil and a $Li(Ni_{0.4}Mn_{0.4}Co_{0.2})O_2$ (NMC422) cathode with an areal capacity of 1.75 mAh cm^{-2} retained ~97.1% capacity retention after 500 cycles at 1 C charge-discharge rate when the cell was cycled in a mixed salt (0.6 M LiTFSI + 0.4 M LiBOB + 0.05 M $LiPF_6$) carbonated-based liquid electrolyte. Although energy-dense LMBs reported in the literature can achieve a relatively decent cycle life, typically very low charge C-rates, such as C/3 to C/10, are applied.[18,28,50,53,54] Few energy-dense LMBs can be stably cycled at a high charge C-rate (such as $\geqslant$ 1 C), limited by the liquid electrolyte properties (e.g., low ionic conductivity)[32,34,39,47] and/or low Li CE at high current density.

In this work, we build on our previous work by employing $Li(Ni_{0.8}Co_{0.1}Mn_{0.1})O_2$ (NMC811) as the cathode material, which possesses higher specific capacity and lower Co content relative to NMC622.[58] We present a LMB which can achieve an energy density of ~350 Wh kg^{-1} in pouch cell format by using a high areal capacity NMC811 cathode and a Li metal anode with minimal excess (N/P ratio $\leqslant$3.1). We then demonstrate the cycling stability of such energy-dense LMBs at high charge rates ($\geqslant$1 C).

Experimental

Electrolyte preparation.—Battery-grade LiFSI salt , DME solvent, trially phosphate (TAP) additive were sourced from Nippon Shokubai in Japan, Sigma-Aldrich and TCI American, respectively. 1, 1, 2, 2-Tetrafluoroethyl 2, 2, 3, 3-tetrafluoropropyl ether (TTE) was used as an inert diluent and was obtained from Synquest Laboratories, Incorporated. The electrolyte was prepared using a similar method to that reported in our previous work.[4] Briefly, DME and TTE was mixed and stirred to yield a mixed solvent, and then LiFSI salt was dissolved in the mixed solvent under mechanical stirring followed by the addition of TAP. The final composition of the electrolyte was LiFSI: DME: TTE = 1: 1.2: 3 (denoted as LiFSI-1.2DME-3TTE) with 1 wt. % TAP and the LiFSI concentration in the electrolyte was about 1.5 M. The electrolyte was prepared in an Ar-filled MBraun glove box with an oxygen level of <0.1 ppm and H_2O level of <0.1 ppm.

Coin cell preparation.—Two types of CR2032-type coin cells were used in this work: Li || Cu and Li || NMC811 cells. Thick (250 μm) and thin (50 μm) Li chips were used in the former and latter coin cells, respectively. Li chips with a thickness of 250 μm were obtained from MTI Corporation, USA; while Li foils with a thickness of 50 μm coated on 10 μm Cu foils were purchased from AME Energy Corporation, China. NMC811 electrodes were fabricated with active material loading of 16.5 mg cm^{-2} on 15 μm Al foil. The single Li || Cu coin cell used in this work consisted of a Li chip with a thickness of 250 μm and a diameter of 9 mm, a layer of Celgard-2325 separator with a thickness of 25 μm, and a piece of Cu disc with a thickness of 10 μm and a diameter of 19 mm. Each Li || NMC811 coin cell consisted of a Li foil anode, a layer of Celgard-2325 separator with a thickness of 25 μm, and a NMC811/Al foil disc with a diameter of 14 mm as a cathode. The Li foil anode used in the Li || NMC811 coin cell was a Li disc with a thickness of 50 μm and a diameter of 15–16 mm cut in-house from as-obtained Li foil coated on Cu foil. For each Li || Cu or Li || NMC811 coin cell, approximately 100 μl of the electrolyte was used. The coin cells were also prepared in Ar-filled MBraun glove box. The detailed method for the coin cell preparation can be found in our previous work.[4]

Electrochemical characterization.—All electrochemical tests were carried out with either a Land battery testing system (Model: CT2001A, Wuhan Land, China) or an Arbin battery testing system (Model: BT2000, Arbin, USA). To measure the Li Coulombic efficiency (CE) with a Li || Cu coin cell, Li was first electroplated onto the Cu foil at a prescribed current density to achieve a total plating capacity of 3 mAh cm^{-2}, and then the plated Li was stripped from the Cu foil until a cut-off voltage of −1.0 V was reached. The plating/stripping cycle was repeated for several tens or hundreds of sequential cycles under different current densities and temperatures to determine the Li CE and investigate the cycling stability of Li metal anodes. For fresh Li || NMC811 coin cells, after several formation cycles at room temperature (RT), the charge/discharge performance of the fresh cells was characterized using a C/10 rate in a voltage range of 2.8–4.2 or 2.8–4.3 V at a required temperature (either RT, 40, or 60 °C). For the C/10 performance characterization, an additional constant voltage (CV) step was added to the charging process: during the CV step, cells were kept at a cut-off charge voltage of 4.2 or 4.3 V until a cut-off current corresponding to C/20 was reached. After C/10 performance characterization, the coin cells were cycled at a required C-rate in the voltage range of 2.8–4.2 V or 2.8–4.3 V. For each aging cycle, an additional CV step was also added to the charging process, during which the cells were kept at a cut-off voltage of 4.2 or 4.3 V until a current corresponding to a certain C-rate (such as C/10 or C/3) was reached. The current densities corresponding to all C-rates were calculated based on the actual discharge capacity of each respective fresh coin cell obtained from the C/10 performance characterization. The cycling test was interrupted from time to time for the C/10 performance characterization (as reference performance test) and electrochemical impedance spectroscopy (EIS) testing. The C/10 charge-discharge performance of the aged cells was evaluated using the same method as for the corresponding fresh cells. For the EIS measurement of fresh and aged cells, the cells were fully charged to a cut-off charge voltage (4.2 or 4.3 V) using a C/10 rate and then discharged to 90% state of charge (SoC) using a C/10 rate. The EIS testing was performed using a Modulab testing system (Ameteck Scientific Instrument, USA) with a frequency range of 1 M to 0.01 Hz and ac amplitude of ±5 mV.

Results and Discussion

Temperature effect on the performance of fresh Li || NMC811 coin cells.—Increasing temperature can enhance the ionic conductivity and Li-ion diffusion coefficient of HCEs, facilitate the kinetics of electrode reactions, and promote the Li solid diffusion in cathode active material particles,[3,34,42,59] which are all beneficial to fast charging of LMBs, particularly in ether-based HCEs. However, at elevated temperatures, ether-based HCEs in contact with NMC become unstable at high voltages.[4] Our recent work demonstrated that a small amount (typically 1 wt. %) of TAP significantly enhances the cycling stability of LMBs with high-voltage NMC622 cathodes.[4] Consequently, in this work, TAP is employed as an additive in the localized ether-based electrolyte (LiFSI-1.2DME-TTE) to enhance the electrolyte stability and cycling stability of LMBs with high-voltage NMC811 cathodes.

First, the temperature effect on the performance of fresh LMBs was investigated. Figure 1 shows the performance of fresh Li (50 μm thick) || NMC811 coin cells under C/10 charge/discharge at RT, 40, and 60 °C. At RT, the cell delivered a C/10 discharge capacity of ~204 and ~181 mAh g^{-1} when cut-off charge voltage was 4.3 and 4.2 V, respectively. When operation temperature was increased from RT to 40 °C, the C/10 discharge capacity delivered by the cell increased to ~218 and 194 mAh g^{-1} for charge cut-off voltages of 4.3 and 4.2 V, respectively, which was about 7% higher than that at RT. When the operating temperature was further increased to 60 °C, the C/10 discharge capacity increased to ~223 and ~201 mAh g^{-1} for charge cut-off voltages of 4.3 and 4.2 V, respectively. This indicates that compared with RT, the cell can deliver at least 9.3% higher capacity and energy density at 60 °C. The high discharge capacity and energy density at elevated temperature is attributed to enhanced ionic conductivity and Li ion diffusion coefficient of HCEs, reduced electrolyte viscosity, fast kinetic of electrode reactions at electrode/electrolyte interfaces and promoted Li solid diffusion in NMC811 particles [3,34,42,59]

Figure 2 shows a comparison of the impedance spectra of fresh Li (50 μm thick) || NMC811 coin cells under 90% state-of-charge

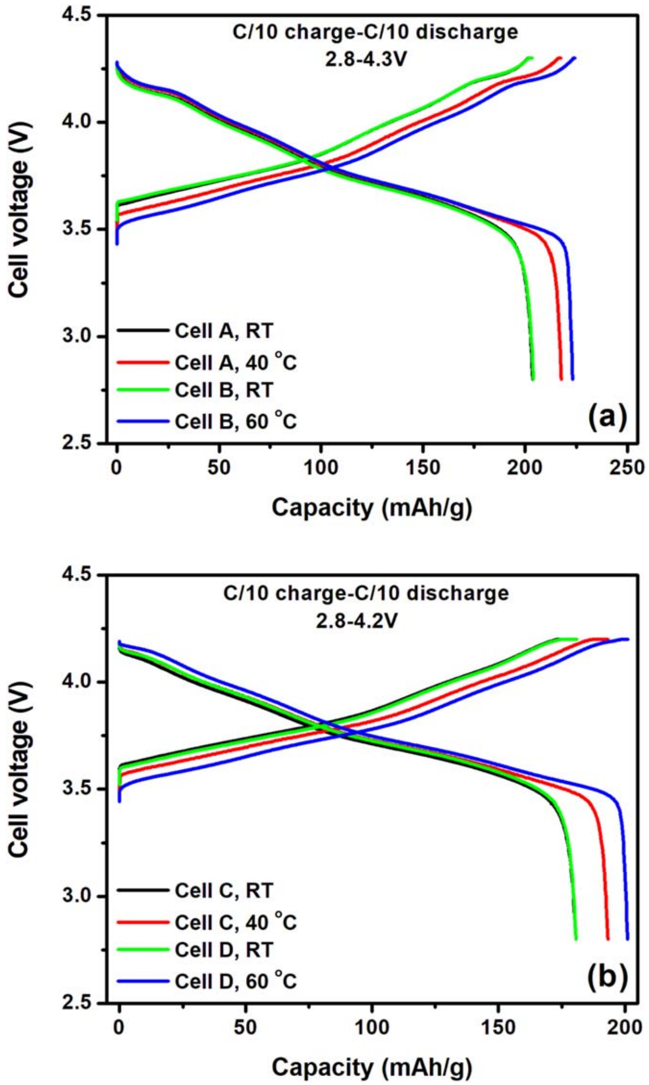

Figure 1. Effect of temperature on the performance of fresh Li (50 μm thick) || NMC811 cells under C/10 charge/discharge in the voltage range of (a) 2.8–4.3 V, and (b) 2.8–4.2 V.

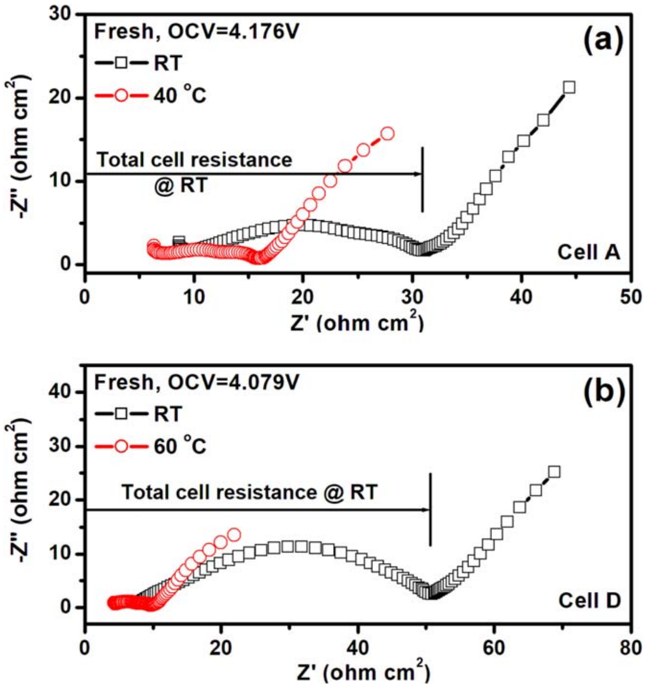

Figure 2. Effect of temperature on the impedance of fresh Li (50 μm thick) || NMC811 cells: (a) Cell A after two formation cycles at 40 °C, full charge to 4.3 V, and discharge to 90% SoC (OCV = 4.176 V); and (b) Cell D after two formation cycles at 60 °C, full charge to 4.2 V, and then discharge to 90% SoC (OCV = 4.079 V).

(SoC) at RT and elevated temperature (40 or 60 °C). Note that the total cell resistance (excluding the line attributed to diffusion) at RT varies between the two cells (Figs. 2a and 2b) in spite of their identical cell components and materials. This variation results from testing at different temperatures (40 and 60 °C) prior to the impedance tests (i.e., formation cycles). For Cell D shown in Fig. 2b, the total cell resistance was ~50.8 ohm cm^2 at RT, exceeding that of Cell A shown in Fig. 2a (~30.9 ohm cm^2), which is due to enhanced decomposition of the ether-based electrolyte at higher temperatures during formation cycles and C/10 performance characterization. However, for both cells, with increasing operating temperature, the total cell resistance substantially decreases. For Cell A, the total cell resistance was ~15.9 ohm cm^2 at 40 °C, almost half of that at RT. While for Cell D, the total cell resistance decreased by ~81% from ~50.8 to 9.7 ohm cm^2 when the temperature was increased from RT to 60 °C. The substantial decrease in total cell resistance at elevated temperatures is mainly due to enhanced ionic conductivity of HCEs as well as fast kinetics of electrode reactions at electrode/electrolyte interfaces.[3,34,42,59] low cell resistance at elevated temperatures is key to enable fast charging of LMBs in ether-based electrolytes.

Effect of temperature and current density on Li Coulombic efficiency.—Li Coulombic efficiency (CE) is a crucial factor that influences the cycle life of LMBs. Li Coulombic inefficiency (CIE) (CIE = 1 − CE) is indicative of the rate at which the Li metal anode is consumed. Li CE (or CIE) is especially important when Li metal anodes of limited excess Li (i.e. 20–50 μm thickness) or Li-free anodes are used.[28,60,61] In the literature, most CE tests are performed under low current density ($\leqslant$1 mA cm^{-2}) and low plating capacity ($\leqslant$2 mAh cm^{-2}). Here, we perform Li CE tests at more practical levels with 3 mAh cm^{-2} plating capacity and current densities up to 9 mA cm^{-2}. Figures 3 and S1 (available online at stacks.iop.org/JES/168/060548/mmedia) show CE evolution with cycle number at different current densities (i.e. C-rate) and two different temperatures (RT and 60 °C) measured in a Li (250 μm thick) || Cu cell in the localized ether-based HCEs. 3 mAh cm^{-2} was chosen for plating capacity as it is close to the areal capacity of NMC811 cathodes used in this work. As shown in Figs. 3a and S1b, the CE was quite stable at 1 mA cm^{-2} (i.e. C/3-rate) and RT for at least 400 cycles. After that, Li plating/stripping cycling was performed for another 100 cycles at 3 mA cm^{-2} (i.e. 1C-rate) and RT. Stable CE was achieved at 1 C and RT (Fig. S1c) except for large fluctuation in CE during the last several cycles. This is mainly due to the formation/growth of Li dendrite at 1C-rate and RT which results in soft internal shorting. When operating temperature was increased to 60 °C, this fluctuation disappeared with continuous cycling at the same current density. Temperature dependence of Li nucleation and growth behavior was investigated by Yan et al.[62] They found that increasing Li deposition temperature results in large nuclei size, low nucleation density, and compact growth of Li metal, avoiding the formation/growth of Li dendrites at high temperature. Their study also showed that this dendrite-free Li growth behavior is mainly due to the enhanced lithiophilicity and the increased Li-ion diffusion coefficient in aprotic electrolytes at high temperature. Li et al.[63] reported that self-heating of the dendrites induced by high current density operation can trigger extensive surface migration of Li, which heals the dendrites and smoothens the Li metal surface. In this work, it similarly appears that Li dendrites formed at room temperature are dissolved by continuous plating/stripping cycling at elevated

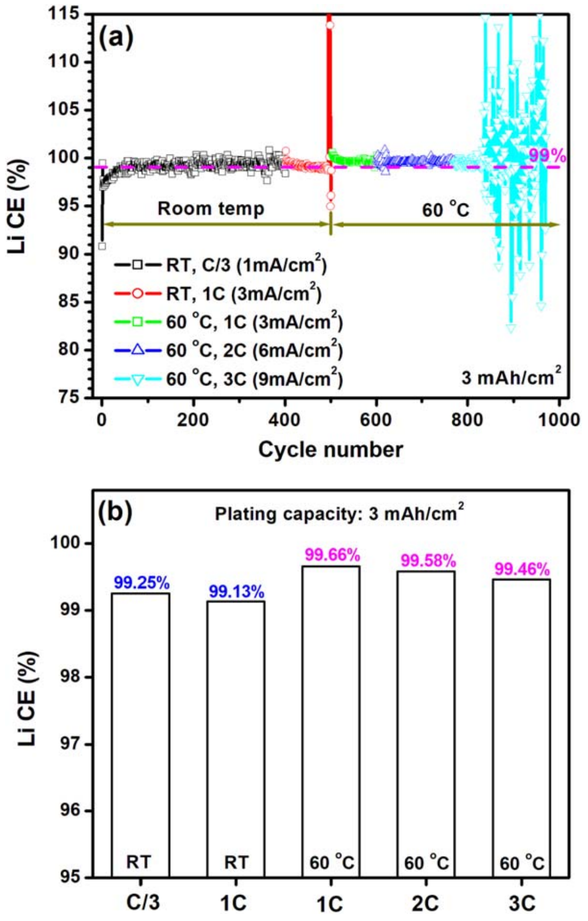

Figure 3. (a) Stability of Li Coulombic efficiency (CE) with cycling and (b) CE as a function of temperature and plating/stripping current densities (i.e. C-rate) measured in Li || Cu cells in LiFSI-1.2DME-3.0TTE electrolyte with 1 wt.% TAP. The total plating capacity for each cycle is kept constant at 3 mAh cm^{-2}, and the plating/stripping current densities vary with cycling during the whole test: C/3–1 mA cm^{-2}, 1 C–3 mA cm^{-2}, 2 C–6 mA cm^{-2}, and 3 C–9 mA cm^{-2}.

temperatures. At 60 °C, stable CE was achieved for $\sim$98, $\sim$167 and $\sim$65 cycles at 3, 6, and 9 mA cm^{-2} (i.e. 1 C, 2 C, and 3C-rate), respectively. However, after $\sim$65 cycles at 9 mA cm^{-2}, the CE became unstable with a large fluctuation, which may also be due to the formation/growth of Li dendrite at 3C-rate and thus soft internal shorting. Figure 3b shows the average Li CE from the cycles with stable CE at different plating/stripping current densities and temperatures. At RT, with an increase in current density from C/3 (i.e. 1 mA cm^{-2}) to 1 C (3 mA cm^{-2}), the Li CE slightly decreased from 99.25 to 99.13%. A similar phenomenon was observed for the Li CE at 60 °C where the Li CE decreased from 99.66 to 99.58 and 99.46% when the plating/stripping current density was increased from 1 C to 2 C and 3 C, respectively, as shown in Figs. S1d–f. This is mainly due to smaller particle size of Li deposited at higher current density, which augments the electrolyte/electrode interfacial area and decreases the CE. Moreover, at the same current density of 3 mA cm^{-2} (i.e. 1C-rate), when increasing temperature from RT to 60 °C, Li CE jumped from 99.13 to 99.66% and corresponding Li Coulombic inefficiency significantly decreased from 0.87 to 0.34%, respectively. Cui's group[64] also reported that the average Li CE increases with elevating temperature in some liquid electrolytes. Since Li ion mass transport is enhanced at elevated temperatures, the formation/growth of Li dendrites is suppressed and large size Li particles are deposited, shrinking the electrolyte/electrode interfacial area and increasing the Li CE.[4,64] As mentioned, Li CIE is an indicator of consumption rate of Li metal, which significantly affects the cycle life of LMBs (Fig. S2). Thus, with decreasing CIE, the number of equivalent full cycles (EFCs) (vs C/10 discharge capacity for a fresh cell) significantly increases. In a conventional liquid electrolyte such as 1 M LiPF$_6$ in EC/EMC (3:7 wt. %) + 2% VC, Li CE is lower than 90% (CIE $>$10%),[4] indicating that LMBs in the conventional liquid electrolyte can achieve only several to several tens of EFCs, depending on N/P ratio (i.e. the ratio of the capacity of a Li anode to that of a cathode). In this work, as shown in Fig. 3b, a Li CE of $>$99% (CIE $<$ 1%) can be achieved in our ether-based HCEs. This implies that several hundreds of EFCs could be achieved for a LMB with an N/P ratio of 2–3 cycled in our ether-based HCEs. Additionally, high Li CEs of 99.66%–99.46% and low corresponding CIEs of 0.34%–0.64% were achieved even at high C-rates (1 C to 3 C) and 60 °C. These results are promising for achieving stable cycling and fast-charging capability of energy dense LMBs (i.e., LMBs with minimal excess Li anodes and high areal capacity ($\geqslant$3 mAh cm^{-2}) NMC811 cathodes).

Figures 4a and 4b depict the voltage profiles of the Li (250 μm thick) || Cu cell during select plating/stripping cycles of the Li CE testing discussed for Fig. 3. During the plating step, Li is stripped from the Li chip and then plated onto the Cu foil substrate; while during the stripping step, Li is stripping from the Cu foil substrate and then plated back to the Li chip. Both the steps include a Li plating process at one electrode and a Li stripping process at another electrode simultaneously. As one can see, the voltage profile for the plating step should be symmetric with that for the stripping step, and the overpotential (η) during both the steps should be approximately the same, which is similar to our work previously reported.[4] Therefore, η can be extracted as half of the difference in voltage profiles between two steps, as labeled in Figs. 4a and 4b. Figure 4c shows the overpotential located at a plating capacity of 1.5 and 3.0 mAh cm^{-2} as a function of cycle number at different C-rates and temperatures. At RT, the overpotential located at a plating capacity of 1.5 mAh cm^{-2} decreased from the 5th to 100th cycle due to cell activation and then was kept nearly constant for about 300 cycles. A similar phenomenon was observed for the overpotential at a plating capacity of 3.0 mAh cm^{-2}. These results indicate that Li metal electrode can be stably cycled at C/3-rate for $\geqslant$400 cycles at RT. When current density was increased from C/3 to 1 C rate at RT, the overpotential corresponding to the plating capacity of 1.5 mAh cm^{-2} increased from 83.8 to 240.6 mV, while the overpotential for plating capacity of 3.0 mAh cm^{-2} increased from 197.8 to 396.2 mV. Such a high overpotential at 1C-rate and RT indicates that it is difficult, if possible at all, to achieve stable cycling of LMBs with a fast charge C-rate (such as $\geqslant$1 C) at RT. Note that there was a sudden decrease in the overpotential at 1 C for the plating capacity of 3.0 mAh cm^{-2} (also shown in Fig. 4a) when cycle number increased from 450 to 500 cycles at RT, which is due to possible soft shorting causing by the formation/growth of Li dendrites during the high C-rate (1 C) plating process at RT. The issues associated with fast-charging at RT can be alleviated by elevating the temperature to e.g. 60 °C, supported by the significant reduction in the overpotential for Li plating/stripping process as compared to that at the same C-rate and RT. Specifically, an operating temperature increase from RT to 60 °C provided a $\sim$3.2-fold reduction ($\sim$243 to $\sim$75 mV) in the overpotential at 1C-rate for the plating of 1.5 mAh cm^{-2}. Moreover, the overpotentials at 2 C and 3C-rate for plating of 1.5 mAh cm^{-2} were $\sim$106 and $\sim$137 mV at 60 °C, respectively, which are comparable with that at C/3-rate at RT. Similar to the effect of temperature on impedance, this result is attributed to increased Li ion conductivity, fast Li plating/stripping process and enhanced Li-ion diffusion. However, at a plating capacity of 3.0 mAh cm^{-2} and 60 °C, the overpotentials at 2 C and 3C-rate were $\geqslant$300 mV. Such high overpotentials could hinder stable, high-capacity cycling of LMBs in our ether-based HCEs at a charge C-rate higher than 2 C and 3 C.

Cycling test of Li || NMC811 coin cells under low C-rate at RT and 40 °C.—Figure 5a shows the cycling performance of Li ||

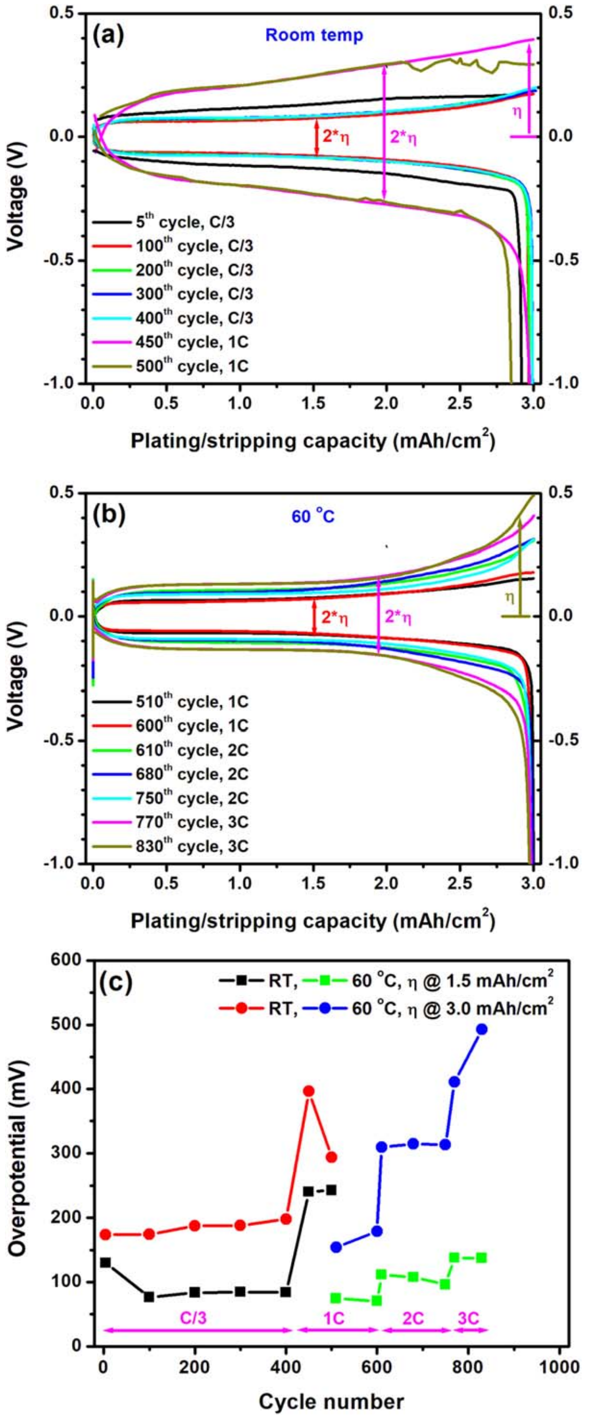

Figure 4. (a), (b) Voltage profiles of selected Li plating/stripping cycles at (a) room temperature and (b) 60 °C, and (c) overpotential (η) for plating capacity of 1.5 and 3.0 mAh cm^{-2} as a function of cycle number for Li (250 μm thick) || Cu cells in LiFSI-1.2DME-3.0TTE electrolyte with 1 wt. % TAP. The total plating capacity for each cycle is kept the same (3 mAh cm^{-2}), and the plating/stripping current densities vary with cycling during whole test: C/3–1 mA cm^{-2}, 1 C–3 mA cm^{-2}, 2 C–6 mA cm^{-2}, and 3 C–9 mA cm^{-2}. Overpotential (η) is related to Li plating/stripping process.

NMC811 coin cells with 50 μm thick Li foil at both RT and 40 °C. The cells were cycled between 2.8 and 4.3 V at C/3-C/3 charge-discharge rates. At RT, the C/3 discharge capacity quickly decreased with cycle number. At RT, the CE was quite stable with an average CE of ~99.88% within 100 cycles, but the cell achieved only 100 cycles at a C/3 capacity retention of 80%. When temperature was increased from RT to 40 °C, the cell not only achieved higher initial C/3 discharge capacity (3.381 mAh cm^{-2} at 40 °C vs 3.066 mAh cm^{-2} at RT), the cycle life also improved. At 40 °C, the cell achieved ~208 and ~373 cycles at a C/3 capacity retention of 80% and 70%, respectively, which was almost double the cycle life at RT. Also, the CE was quite stable for at least 400 cycles with a CE of ~99.79% when averaged over the first 400 cycles excluding all C/10 charge/discharge cycles and the first C/3 charge/discharge cycle after each reference performance test. Generally, LiFSI salt is believed to cause Al current collector corrosion in a dilute LiFSI-based electrolyte.[32,36] However, increasing the LiFSI/DME molar ratio (i.e., salt concentration) can effectively passivate the surface of Al current collector and prevent apparent Al corrosion at high voltage.[32,36] For example, Ren et al.[36] found that there is no apparent Al corrosion when Al foil is held at 4.4 V at 25 °C for 7 days in the LiFSI-1.4DME electrolyte. Based on our experience and previously reported work,[4] we haven't met any problem related to apparent Al corrosion and overcharge during cycling test of Li || NMC622 coin cells in a voltage window of 2.5–4.3 V for several hundreds of cycles in highly concentrated electrolytes. Therefore, the corrosion of Al foil current collector is not a concern for cycling test of Li || NMC811 coin cells in this work.

Figures 5b and 5c show C/10 charge/discharge curves of Li || NMC811 coin cells after various cycle numbers for cycling at RT and 40 °C, respectively. For the same cycle number (e.g. 200 cycles), the cell cycled at 40 °C displayed both smaller capacity fade and less voltage fade than that of the cell cycled at RT. The C/10 capacity retention as a function of cycle number for both cases was plotted in Fig. 5d for a comparison. The cell can achieve ~140 and ~371 cycles at a C/10 capacity retention of 80% at RT and 40 °C, respectively. At 40 °C and after 445 cycles, the cell accumulated a total discharge capacity of 1223 mAh cm^{-2} (very close to the accumulated charge capacity due to very high average cell efficiency of 99.79%), while the accumulated loss of capacity of Li inventory (the sum of the full capacity of Li foil and the C/10 capacity loss of the NMC811 cathode) was $\leqslant$11.45 mAh cm^{-2}. Therefore, the Li CIE during the whole cycling test was calculated to be $\leqslant$0.94%, which corresponds to an estimated Li CE of $\geqslant$99.06%. This result is close to the Li CE observed for the Li || Cu coin cell as shown in Fig. 3. As shown in Figs. 1 and 2, operating temperature has a significant impact on C/10 discharge capacity and cell impedance of fresh Li || NMC811 coin cells. Such an impact becomes more significant for high C-rate (such as C/3) discharge capacity during cycling. Moreover, the porous SEI layer formed on the surface of Li metal anode becomes thicker with cycling due to the side reaction of Li metal and electrolyte, making temperature have much more significant effect on the discharge capacity, especially for high C-rate such as C/3. Therefore, even for the cells with the SEI layer of the same thickness on Li metal anode, the cell discharge capacity (especially for C/3) decays at a faster rate at RT than that at 40 °C. This is why we observed that the cycle life prolonged with increasing temperature for the same cells.

Figures 6a and 6b show the impedance of fresh and aged Li (50 μm thick) || NMC811 coin cells cycled at RT and 40 °C, respectively. It is found that the cell resistance for both cases significantly increased with cycling. In the case of the cell cycled at RT, the total cell resistance (excluding the linear part due to mass transport resistance) measured at RT increased from ~27 ohm cm^2 for the fresh cell to ~60 ohm cm^2 for the cell aged for 200 cycles. In the case of the cell cycled at 40 °C, the total cell resistance measured at 40 °C increased from ~16.2 ohm cm^2 for the fresh cell to ~38.1 and 104.2 ohm cm^2 for the aged cell after 200 and 400 cycles, respectively. The significant increase in total cell resistance with cycling is attributed to the growth of surface film on the NMC811 cathode, increase in charge-transfer resistance, and formation/growth of thick and porous SEI layer on the surface of Li foil.[53,55] The increased cell resistance with cycling leads to growing rate-dependence of capacity as the cell ages (e.g., the difference of

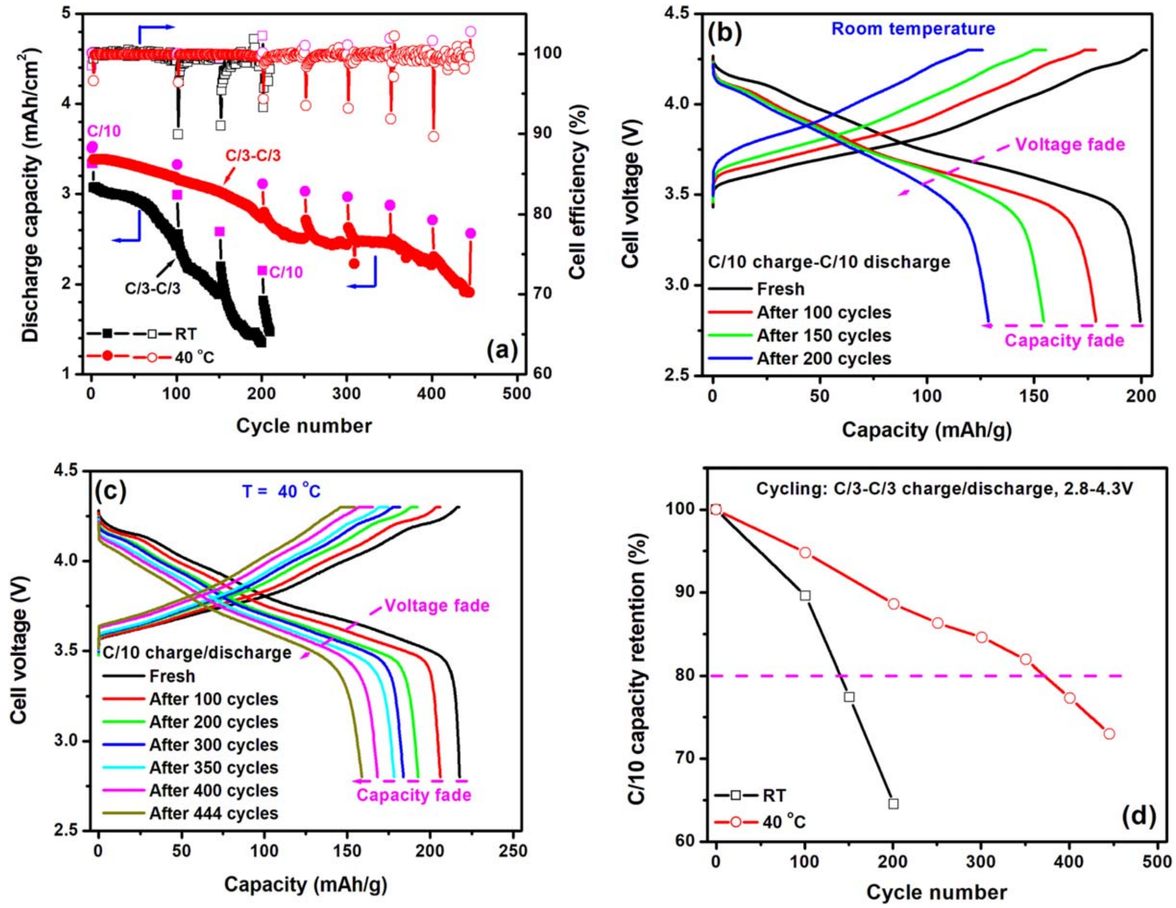

Figure 5. (a) Cycle performance, (b), (c) C/10 charge/discharge curves (voltage vs capacity) at (b) room temperature (RT) and (c) 40 °C, and (d) C/10 capacity retention of Li (50 μm thick) || NMC811 cells as a function of cycle number. The cells were cycled under C/3-C/3 charge-discharge with a voltage range of 2.8–4.3 V at RT and 40 °C, respectively. Note that the magenta spike data points in Fig. 5a are for C/10 charge/discharge during reference performance tests.

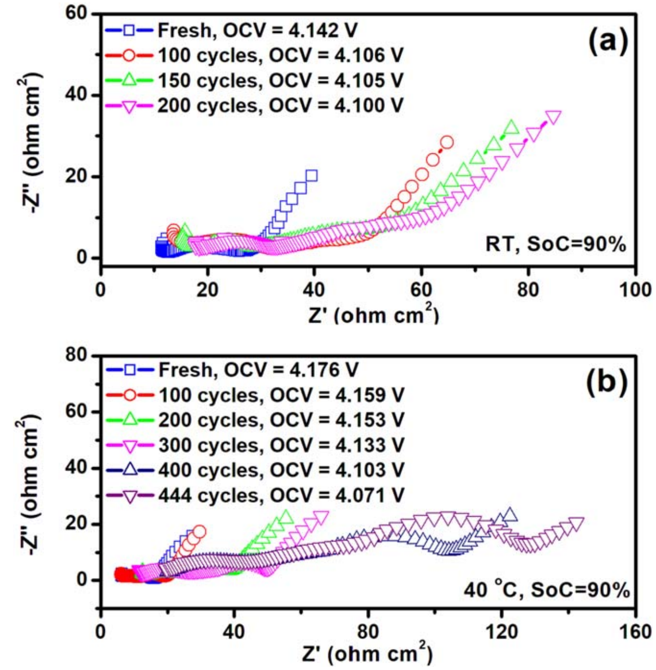

Figure 6. Impedance as a function of cycle number of fresh and aged Li (50 μm thick) || NMC811cells: (a) cycled at room temperature (RT) and (b) cycled at 40 °C. The cells were cycled under C/3-C/3 charge-discharge with a voltage range of 2.8–4.3 V.

capacity fade between at C/3 and C/10 charge/discharge at the same cycle, as shown in Fig. 5a). For example, the cell cycled at 40 °C displayed a C/3 capacity retention of ~80.9 and ~72.5% after 200 and 350 cycles, respectively. At the same cycle numbers and a lower C-rate of C/10, the capacity retention increased to ~88.6 (7.7% higher) and ~81.9% (9.4% higher).

Cycling test of Li || NMC811 coin cells under fast charge rate at elevated temperature.—Figure 7 depicts the discharge capacity and CE as a function of cycle number for Li (50 μm thick) || NMC811 coin cells cycled at 40 and 60 °C with different charge C-rates and a voltage range of 2.8–4.2 V. As shown in Fig. 5a, the cells can achieve ~208 and ~373 cycles at a C/3 capacity retention of 80% and 70%, respectively, when the cell was cycled at low C-rate such as C/3 and 40 °C. However, when the charge/discharge C-rate was increased to 1 C (1 C = 3.15 mA cm^{-2}), the cycling performance of the cell at 40 °C became poor with a fast capacity drop after ~80 cycles. The cell achieved only ~80 cycles at 1 C capacity retention of 80% when cycled at 1 C charge/discharge rate and 40 °C. After 101 cycles, 1 C discharge capacity dropped to 1.492 mAh cm^{-2}, which was about half of that of the fresh cell (i.e., 2.799 mAh cm^{-2}). However, when the charge/discharge C-rate was switched back to C/10, the cell can still deliver a C/10 discharge capacity of ~2.843 mAh cm^{-2}, which was only 9.8% loss from that of the fresh cell (i.e. 3.151 mAh cm^{-2}). A similar phenomenon was also observed by Lu et al.[55] The large difference between 1 C and C/10 capacity loss is believed to be attributed to the quick formation/growth of a highly resistive SEI layer on Li foil and thus a significant increase in cell impedance when the cell is cycled at a high current density.[55] Moreover, in the case of the cell cycled at 1 C

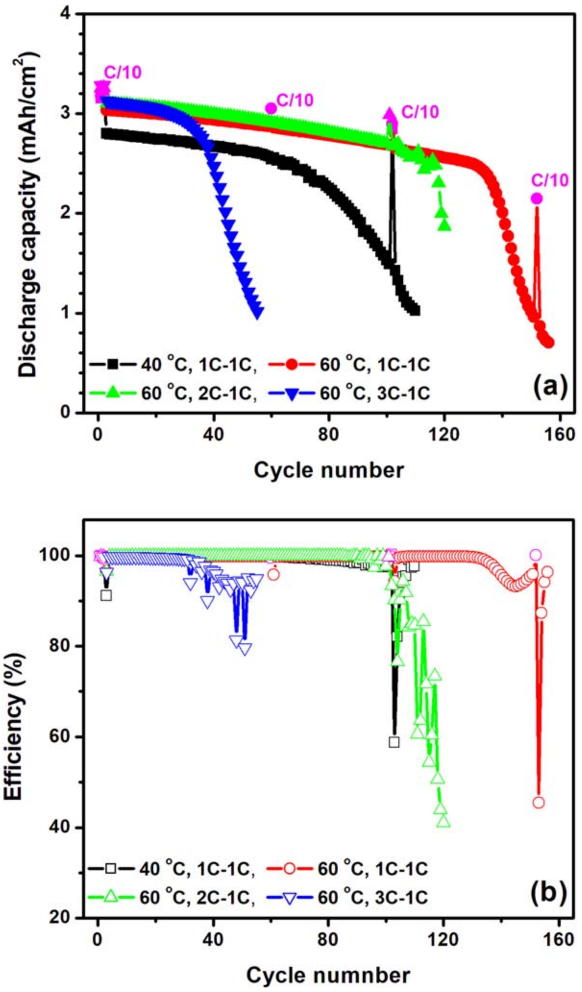

Figure 7. (a) Discharge capacity and (b) Coulombic efficiency as a function of cycle number for Li (50 μm thick) || NMC811 cells. The cells were cycled under different charge/discharge C-rates in the voltage range of 2.8–4.2 V at 40 and 60 °C, respectively. Please note that the magenta spike data points in Fig. 7a are for C/10 charge/discharge during reference performance tests.

charge/discharge C-rate and 40 °C, the CE remains quite stable CE for ~70 cycles with an average CE of ~99.69% and then CE gradually decreased with cycling during subsequent cycles (Fig. 7b). When operating temperature was increased from 40 to 60 °C, the cell not only achieved higher discharge capacity for the fresh cell but also showed better cycling performance at 1 C charge/discharge rate. At 60 °C, the cell achieved a 1 C discharge capacity of ~3.034 mAh cm^{-2}, ~8.4% higher than that at 40 °C. Moreover, the cell achieved ~133 cycles at a 1 C capacity retention of 80% when cycled at a 1 C charge/discharge rate and 60 °C, a ~66% increase over the ~80 cycles observed for the same C-rate and 40 °C. The higher discharge capacity for the fresh cell and improved cycling performance at 60 °C is due to higher Li CE (Fig. 3), lower cell impedance (Fig. 2), and smaller overpotential related to the Li plating/stripping process (Fig. 4). In addition, in the case of the cell cycled at 1 C charge/discharge C-rate and 60 °C, the cell can achieve a quite stable CE for ~130 cycles (~99.76% CE on average). However, after 130 cycles, the CE also decreased with further cycling, which may be due to soft internal shorting.

For practical use (e.g., electric vehicles), it is important to investigate the cycling behavior of energy-dense LMBs at a charge C-rate higher than 1 C. As shown in Fig. 7, when the charge C-rate during cycling was increased from 1 C to 2 C and 3 C while operating temperature and discharge C-rate were kept the same (i.e. 60 °C and 1 C), the cycling performance of the Li (50 μm thick) || NMC811 coin cells worsened. The cells achieved ~117 and ~39 cycles at 1 C capacity loss of 20% for 2 C and 3 C charge C-rate, respectively. Similar to the cases of 1 C charge rate at 40 and 60 °C, 2 C and 3 C charge C-rate cycling at 60 °C resulted in a rapid capacity decay during the final stages of cycling. During the earlier stages of cycling (~100 and ~30 cycles for 2 C and 3 C charge C-rate), the CE was quite stable, representing an average CE of ~99.83 and ~99.56%, respectively (Fig. 7b). However, in the last phase of the cycling test for both cases, the CE decreased quickly, which is probably due to soft internal shorting caused by the formation/growth of Li dendrites and explains the rapid capacity loss.

Figures 8a–8c show the C/10 charge/discharge curves of fresh and aged Li (50 μm thick) || NMC811 coin cells cycled under two different charge/discharge C-rates (1C-1C and 2C-1C) and at two different temperatures (40 and 60 °C). The C/10 capacity retention as a function of cycle number for these cases is plotted in Fig. 8d. Both capacity fade and voltage fade were observed for all three cases: (a) 40 °C and 1C-1C, (b) 60 °C and 1C-1C and (c) 60 °C and 2C-1C. The C/10 capacity retention follows almost the same trend and remains >90% for all three cases within 102 cycles (Fig. 8d). Based on the average Li CE of >99% (Fig. 3) and the total accumulated discharge capacity of ~253, ~295, and ~299 mAh cm^{-2} for ~102 stable cycles, the corresponding capacity of Li consumed was calculated to be <2.53, 2.95 and 2.99 mAh cm^{-2} in the case of (a) 40 °C and 1C-1C, (b) 60 °C and 1C-1C, and (c) 60 °C and 2C-1C, respectively, which represent only 25%-30% of the total areal capacity of Li foil anode with a thickness of 50 μm (~10.5 mAh cm^{-2}). Thus, after 102 cycles, there was still excess Li available at the anode, and the C/10 capacity loss within 102 cycles is due to the capacity loss of NMC811 cathodes as well as the effect of voltage fade caused by the increase in cell resistance. However, in the final stage of cycling at 60 °C and 1C-1C, the C/10 capacity retention decreased sharply from ~91.1% to ~67.4% from 102 to 152 cycles. This is mainly due to the formation of thick porous SEI layer on Li foil, electrolyte dry-out/transport limitation, and significantly increased cell resistance. When comparing the C/10 charge/discharge curve between the fresh and aged cells after cycling for ~100 cycles, it was found that the voltage fade followed the following order: 1C–1C at 40 °C > 2C–1C at 60 °C > 1C–1C at 60 °C. This difference in voltage fade is originated from the different cell impedance. Clearly cycling at higher charge C-rate leads to fast growth of porous SEI layer on Li foil and thus high cell impedance, an effect that is exacerbated at lower temperatures.

To gain some meaningful insight into the failure mechanism of LMBs cycled at high C-rate, we disassembled the cell aged for 156 cycles at 1C-1C and 60 °C (Fig. S4) in a glove box and reconstructed two coin cells from the aged electrodes (Fig. 9). One reconstructed cell consisted of the aged Li foil and a fresh Cu foil filled with fresh HCE while the another cell consisted of a fresh Li foil (50 μm thick) and the aged NMC811 cathode in a fresh HCE. As shown in Fig. S4, a thick and loosely adhered layer with a dark color was observed on the Li foil, which was easily detached from the Li foil and attached to the separator. This layer is assumed to be the porous SEI layer due to the reaction of Li metal and electrolyte. In the area of the anode where the SEI layer was detached, the unused Li foil can be observed. The surface of NMC811 cathode seems smooth without any damage noticeable to the naked eye. The side of the separator towards the Li metal anode appeared to contain some debris due to the attachment of the SEI layer, while the side that faced the NMC811 cathode looked quite clean. From the re-constructed Li || Cu coin cell, we obtained the capacity of the remaining Li foil of 13.0 mAh (Fig. 9a). The loss in areal capacity of Li foil (Q_{loss}) can be calculated based on Eq. 1, where $S_{\text{Li foil}}$ and S_C are the area of Li foil with a diameter of 15.5 mm and the area of NMC811 cathode with a diameter of 14 mm, respectively. The calculated loss in areal capacity of Li foil is 4.42 mAh cm^{-2}, which is ~42% of the original capacity of Li foil with a thickness of 50 μm. Since the total

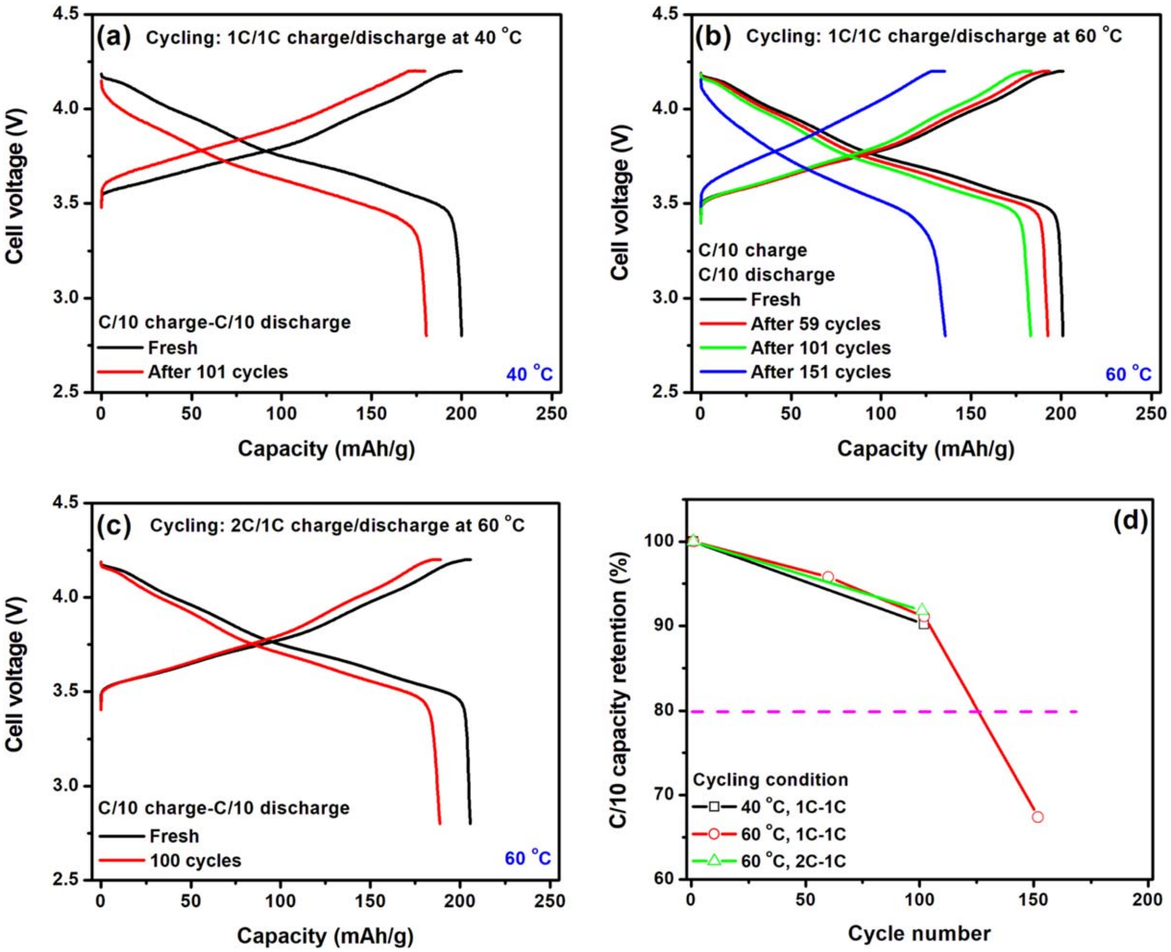

Figure 8. C/10 charge/discharge curve (voltage vs capacity) of fresh and aged Li (50 μm thick) || NMC811 cells cycled under different charge/discharge rates in the voltage range of 2.8–4.2 V at different temperatures: (a) 1C-1C at 40 °C, (b) 1C-1C at 60 °C, and (c) 2C-1C at 60 °C; and (d) C/10 capacity retention of the cells as a function of cycle number.

accumulated discharge capacity was ~410 mAh cm^{-2} over 156 cycles, the Li CIE can be calculated to be ~1.08%, and corresponding Li CE was ~98.92%, which was close to the value measured with Li || Cu coin cells (Fig. 3). On the other hand, the reconstructed cell consisting a fresh Li foil (50 μm thick) and the aged NMC811 cathode with fresh HCE showed very poor performance, as shown in Fig. 9b. The cell delivered only ~80 and 101 mAh g^{-1} at a C/10 and C/20-rate, respectively, which were much lower than that of a fresh cell shown in Fig. 1b (201 mAh g^{-1} at C/10-rate). This indicates that the cathode performance significantly decays with cycling, especially in the final stage. The degradation of NMC811 cathode may be due to the formation/growth of highly resistive films on the surface of NMC811 cathode caused by the decomposition of the electrolyte at high voltage and high temperature, which results in severe mass transport limitation.

$$Q_{\text{loss}} = (10.5\ \text{mAh cm}^{-2} * S_{\text{Li foil}} - 13.0\ \text{mAh})/S_{\text{C}} \quad [1]$$

To further increase the cycle life of LMBs, we shortened the exposure time to high voltage by increasing the cut-off current for the constant voltage (4.2 V) charging phase from C/10 to C/3. We also reduced the discharge C-rate from 1 C to C/3 to avoid severe mass transport limitation during the discharge process. Figure 10 shows the cycling performance of a Li (50 μm thick) || NMC811 cell under 1C-C/3 charge-discharge with a voltage window of 2.8–4.2 V at 60 °C. For comparison, the cycling performance of an equivalent cell cycled under 1C-1C charge-discharge rates with the same voltage range and temperature was also plotted. Although there was a slight decrease in initial C/3 discharge capacity due to the CV cutoff current increase, the cycle performance of the cell was enhanced. The cell achieved ~158 and ~189 cycles at a C/3 capacity retention of 80% and 70%, respectively. The cell also achieved a stable efficiency for ~189 cycles with an average efficiency of ~99.86%, which was higher than that of the cell cycled at 1C-1C with a cut-off current of C/10 during the CV step (i.e., ~99.76%). This implies that shortening the time of exposure to high voltage can reduce the amount of electrolyte decomposition and thus enhance the cell cycle life. After ~189 cycles, the cell failed suddenly with a sharp decay in the discharge capacity and a significant decrease in the cell efficiency, which is believed to stem from soft internal shorting caused by the formation/growth of Li dendrites. A practical pouch cell using the same electrode and electrolyte used in this work can achieve an energy density of ~320 and ~350 Wh kg^{-1} at RT and 60 °C, respectively (Table SI). Such an energy-dense cell can stably operate for 158 ~ 189 cycles at a relatively high charge C-rate such as 1 C, outperforming most of reported work in the literature (Table SII).

Conclusions

The cycling stability of energy-dense LMBs with high areal capacity NMC811 cathodes and minimal excess Li metal anodes (N/P ratio of 2.8–3.1) at different charge rates and temperatures was investigated in ether-based HCEs. It is found that the cell can achieve notable cycle performance (200–350 cycles) at a low charge/discharge C-rate (such as C/3) and a moderately elevated temperature (such as 40 °C). However, high charge/discharge C-rate (such as 1 C) is detrimental to the cycle performance at 40 °C. Further

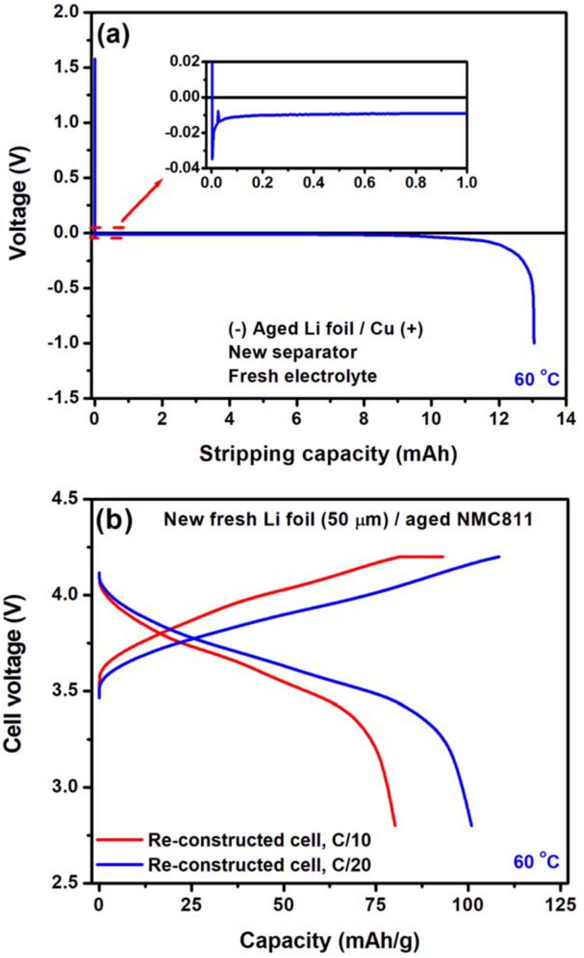

Figure 9. (a) Stripping of the remaining Li foil from an aged cell using a re-constructed Li || Cu cell with aged Li foil, Cu foil, new separator, and fresh electrolyte; (b) Charge-discharge curve of a re-constructed Li || NMC811 cell with fresh Li foil (50 μm), aged NMC811 cathode, new separator, and fresh electrolyte. The aged Li foil and aged NMC811 cathode were collected from the cell after being cycled for 156 cycles (Cycling conditions: 1C-1C charge-discharge, 2.8–4.2 V, and 60 °C, as shown in Figs. 7 and 8).

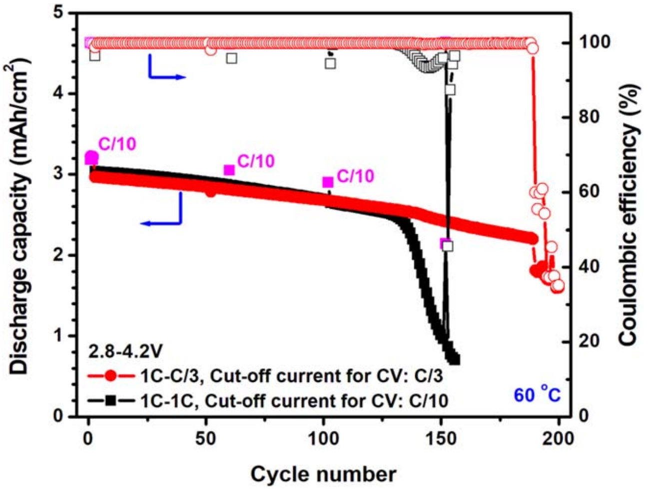

Figure 10. Cycling performance of a Li (50 μm thick) || NMC811 cell under 1C-C/3 charge-discharge with a voltage window of 2.8–4.2 V at 60 °C. For comparison, the cycling performance of the Li (50 μm thick) || NMC811 cell under 1 C charge-1C discharge in the same voltage range at the same temperature was also plotted. Please note that the magenta spike data points are for C/10 charge/discharge during reference performance tests.

elevating the operating temperature to 60 °C enhances the cycle performance for such high charge C-rates, providing stable operation for 158–189 cycles. To further increase cycling stability of energy dense LMBs, an in-depth understanding of the failure mechanisms of LMBs during cycling under fast charging conditions (1 C and even higher) is required to inform the design of an electrolyte with promising properties to meet the key requirements including high Li CE, high ionic conductivity, and high stability at high voltage.

ORCID

Yongjun Leng https://orcid.org/0000-0001-9868-0195
Ryan S. Longchamps https://orcid.org/0000-0002-8168-8032
Chao-Yang Wang https://orcid.org/0000-0003-0650-0025

References

1. Y. Y. Liu, Y. Y. Zhu, and Y. Cui, *Nat. Energy*, **4**, 540 (2019).
2. E. R. Logan and J. R. Dahn, *Trends in Chemistry*, **2**, 354 (2020).
3. X. G. Yang, T. Liu, Y. Gao, S. H. Ge, Y. J. Leng, D. H. Wang, and C. Y. Wang, *Joule*, **3**, 3002 (2019).
4. Y. Leng, S. Ge, R. S. Longchamps, X.-G. Yang, T. Liu, and C.-Y. Wang, *J. Electrochem. Soc.*, **167**, 110543 (2020).
5. X.-G. Yang, T. Liu, and C.-Y. Wang, *Nature Energy*, **6**, 176 (2021).
6. J. Liu et al., *Nat. Energy*, **4**, 180 (2019).
7. X. B. Cheng, R. Zhang, C. Z. Zhao, and Q. Zhang, *Chem. Rev.*, **117**, 10403 (2017).
8. D. C. Lin, Y. Y. Liu, and Y. Cui, *Nat. Nanotechnol.*, **12**, 194 (2017).
9. W. Xu, J. L. Wang, F. Ding, X. L. Chen, E. Nasybutin, Y. H. Zhang, and J. G. Zhang, *Energy Environ. Sci.*, **7**, 513 (2014).
10. C. C. Fang, X. F. Wang, and Y. S. Meng, *Trends in Chemistry*, **1**, 152 (2019).
11. Y. Yamada and A. Yamada, *J. Electrochem. Soc.*, **162**, A2406 (2015).
12. Y. Sun, G. Zheng, Z. W. Seh, N. Liu, S. Wang, J. Sun, H. R. Lee, and Y. Cui, *Chem*, **1**, 287 (2016).
13. D. Lee, S. Sun, J. Kwon, H. Park, M. Jang, E. Park, B. Son, Y. Jung, T. Song, and U. Paik, *Adv. Mater.*, **32**, e1905573 (2020).
14. K. Liu et al., *J. Am. Chem. Soc.*, **139**, 4815 (2017).
15. C. Yang et al., *Proc Natl Acad Sci U S A*, **115**, 3770 (2018).
16. C. P. Yang, Y. X. Yin, S. F. Zhang, N. W. Li, and Y. G. Guo, *Nat. Commun.*, **6**, 8058 (2015).
17. T. T. Zuo, X. W. Wu, C. P. Yang, Y. X. Yin, H. Ye, N. W. Li, and Y. G. Guo, *Adv. Mater.*, **29**, 1700389 (2017).
18. C. Niu et al., *Nat. Nanotechnol.*, **14**, 594 (2019).
19. G. X. Li, Z. Liu, Q. Q. Huang, Y. Gao, M. Regula, D. W. Wang, L. Q. Chen, and D. H. Wang, *Nature Energy*, **3**, 1076 (2018).
20. X. Liang, Q. Pang, I. R. Kochetkov, M. S. Sempere, H. Huang, X. Sun, and L. F. Nazar, *Nature Energy*, **2**, 17119 (2017).
21. Z. Tu, S. Choudhury, M. J. Zachman, S. Wei, K. Zhang, L. F. Kourkoutis, and L. A. Archer, *Nature Energy*, **3**, 310 (2018).
22. M. T. Wan, S. J. Kang, L. Wang, H. W. Lee, G. W. Zheng, Y. Cui, and Y. M. Sun, *Nature Communications*, **11**, 829 (2020).
23. E. Markevich, G. Salitra, and D. Aurbach, *ACS Energy Lett.*, **2**, 1337 (2017).
24. X. Li, J. Zheng, X. Ren, M. H. Engelhard, W. Zhao, Q. Li, J.-G. Zhang, and W. Xu, *Adv. Energy Mater.*, **8**, 1703022 (2018).
25. R. Miao, J. Yang, Z. Xu, J. Wang, Y. Nuli, and L. Sun, *Sci. Rep.*, **6**, 21771 (2016).
26. Z. Yu et al., *Nat. Energy*, **5**, 526 (2020).
27. S. Yuan, J. L. Bao, N. Wang, X. Zhang, Y. Wang, D. G. Truhlar, and Y. Xia, *Chem Commun (Camb)*, **56**, 8257 (2020).
28. Y. Zhu, V. Pande, L. Li, B. Wen, M. S. Pan, D. Wang, Z. F. Ma, V. Viswanathan, and Y. M. Chiang, *Proc Natl Acad Sci U S A*, **117**, 27195 (2020).
29. H. Wang, M. Matsui, H. Kuwata, H. Sonoki, Y. Matsuda, X. F. Shang, Y. Takeda, O. Yamamoto, and N. Imanishi, *Nat. Commun.*, **8**, 15106 (2017).
30. X. Ren et al., *Chem*, **4**, 1877 (2018).
31. Z. Q. Zeng et al., *Nat. Energy*, **3**, 674 (2018).
32. J. Wang, Y. Yamada, K. Sodeyama, C. H. Chiang, Y. Tateyama, and A. Yamada, *Nat. Commun.*, **7**, 12032 (2016).
33. X. Fan et al., *Chem*, **4**, 174 (2018).
34. L. Suo, W. Xue, M. Gobet, S. G. Greenbaum, C. Wang, Y. Chen, W. Yang, Y. Li, and J. Li, *Proc Natl Acad Sci U S A*, **115**, 1156 (2018).
35. S. Jiao et al., *Nat. Energy*, **3**, 739 (2018).
36. X. Ren et al., *ACS Energy Lett.*, **4**, 896 (2019).
37. H. Sun et al., *Adv. Mater.*, **32**, e2001741 (2020).
38. S. Lee, K. Park, B. Koo, C. Park, M. Jang, H. Lee, and H. Lee, *Adv. Funct. Mater.*, **30**, 2003132 (2020).
39. J. F. Qian, W. A. Henderson, W. Xu, P. Bhattacharya, M. Engelhard, O. Borodin, and J. G. Zhang, *Nature Communications*, **6**, 6362 (2015).
40. J. Alvarado et al., *Energy Environ. Sci.*, **12**, 780 (2019).
41. S. Chen, J. Zheng, D. Mei, K. S. Han, M. H. Engelhard, W. Zhao, W. Xu, J. Liu, and J. G. Zhang, *Adv. Mater.*, **30**, e1706102 (2018).
42. P. Li, C. Li, Y. Yang, C. Zhang, R. Wang, Y. Liu, Y. Wang, J. Luo, X. Dong, and Y. Xia, *Research (Wash D C)*, **2019**, 7481319 (2019).
43. Y. G. Lee et al., *Nat. Energy*, **5**, 299 (2020).
44. S. Xin, Y. You, S. Wang, H.-C. Gao, Y.-X. Yin, and Y.-G. Guo, *ACS Energy Lett.*, **2**, 1385 (2017).

45. J. Wan, J. Xie, D. G. Mackanic, W. Burke, Z. Bao, and Y. Cui, *Materials Today Nano*, **4**, 1 (2018).
46. S. Xia, X. Wu, Z. Zhang, Y. Cui, and W. Liu, *Chem*, **5**, 753 (2019).
47. Y. Yamada, J. Wang, S. Ko, E. Watanabe, and A. Yamada, *Nat. Energy*, **4**, 269 (2019).
48. J. Zheng, J. A. Lochala, A. Kwok, Z. D. Deng, and J. Xiao, *Adv Sci (Weinh)*, **4**, 1700032 (2017).
49. K. Ueno, J. Murai, H. moon, K. Dokko, and M. Watanabe, *J. Electrochem. Soc.*, **164**, A6088 (2017).
50. X. D. Ren et al., *Joule*, **3**, 1662 (2019).
51. J. F. Qian, B. D. Adams, J. M. Zheng, W. Xu, W. A. Henderson, J. Wang, M. E. Bowden, S. C. Xu, J. Z. Hu, and J. G. Zhang, *Adv. Funct. Mater.*, **26**, 7094 (2016).
52. R. Weber, M. Genovese, A. J. Louli, S. Hames, C. Martin, I. G. Hill, and J. R. Dahn, *Nat. Energy*, **4**, 683 (2019).
53. C. Niu, H. Lee, S. Chen, Q. Li, J. Du, W. Xu, J.-G. Zhang, M. S. Whittingham, J. Xiao, and J. Liu, *Nat. Energy*, **4**, 551 (2019).
54. A. J. Louli et al., *Nat. Energy*, **5**, 693 (2020).
55. D. Lu et al., *Adv. Energy Mater.*, **5**, 1400993 (2015).
56. H. Xiang, P. Shi, P. Bhattacharya, X. Chen, D. Mei, M. E. Bowden, J. Zheng, J.-G. Zhang, and W. Xu, *J. Power Sources*, **318**, 170 (2016).
57. J. M. Zheng, M. H. Engelhard, D. H. Mei, S. H. Jiao, B. J. Polzin, J. G. Zhang, and W. Xu, *Nat. Energy*, **2**, 17012 (2017).
58. H.-J. Noh, S. Youn, C. S. Yoon, and Y.-K. Sun, *J. Power Sources*, **233**, 121 (2013).
59. X. G. Yang, G. S. Zhang, S. H. Ge, and C. Y. Wang, *Proceedings of the National Academy of Sciences of the United States of America*, **115**, 7266 (2018).
60. J. Qian, B. D. Adams, J. Zheng, W. Xu, W. A. Henderson, J. Wang, M. E. Bowden, S. Xu, J. Hu, and J.-G. Zhang, *Adv. Funct. Mater.*, **26**, 7094 (2016).
61. B. D. Adams, J. Zheng, X. Ren, W. Xu, and J.-G. Zhang, *Adv. Energy Mater.*, **8**, 1702097 (2018).
62. K. Yan, J. Wang, S. Zhao, D. Zhou, B. Sun, Y. Cui, and G. Wang, *Angew. Chem. Int. Ed. Engl.*, **58**, 11364 (2019).
63. B. S. Li Lu, W. Yiping, C. Zhizhong, H. Prateek, W. Baiwei, S. Jian, S. Yunfeng, N. Shankar, and K. Nikhil, *Science*, **359**, 1513 (2018).
64. J. Y. Wang, W. Huang, A. Pei, Y. Z. Li, F. F. Shi, X. Y. Yu, and Y. Cui, *Nat. Energy*, **4**, 664 (2019).